Journal of Glaciology, Vol. 40, No. 134, 1994

Ploughing of subglacial sediment

URS H. FISCHER AND GARRY K. C. CLARKE
Department of Geophysics and Astronomy, University of British Columbia, Vancouver, British Columbia V6T 1Z4, Canada

ABSTRACT. Mechanical conditions at the base of Trapridge Glacier, Yukon Territory, were investigated using a "ploughmeter". We describe the physical characteristics and the theory of this new instrument as well as its operation. Observational results reveal variations in ploughmeter response that might be attributed to spatial variability in subglacial processes or spatial variation in sediment granulometry. Quantitative analysis of the interaction of the ploughmeter with the basal layer yields estimates of rheological parameters. If the sediment is assumed to behave as a Newtonian viscous fluid, the estimated effective viscosity is 3.0×10^9–3.1×10^{10} Pa s; if it is assumed to behave as an ideal plastic solid, the estimated yield strength is 48–57 kPa. In both cases, the estimated shear resistance of subglacial material is comparable to but somewhat less than that required to balance fully the applied basal shear stress.

INTRODUCTION

For a glacier resting on a deformable bed, both sliding and subglacial sediment deformation can contribute to total basal motion (Alley, 1989). Because the operation of these processes depends upon contact conditions at the ice–bed interface, the mechanical and hydrological coupling between a glacier and its bed are topics of interest. However, direct observations of processes at the ice–bed interface remain difficult. Work reported by Kamb and LaChapelle (1964), Boulton and Jones (1979) and Boulton and Hindmarsh (1987) was confined to tunnels in the marginal regions of glaciers. Other investigations of subglacial conditions have been carried out through boreholes drilled to the bed (Engelhardt and others, 1978, 1990a, b; Blake and Clarke, 1989; Kamb and Engelhardt, 1989; Kohler and Proksch, 1991; Blake and others, 1992; Humphrey and others, 1993). Of special relevance to the present study is the work of Humphrey and others (1993), who described an in situ measurement of the strength of deforming subglacial sediment. Their analysis was based on an examination of the plastic deformation of a drill stem that was inadvertently stuck in the bed of Columbia Glacier, Alaska.

At Trapridge Glacier, Yukon Territory, we are examining processes that control partitioning between bottom sliding and sediment deformation by observing how these flow contributions vary spatially and temporally. By simultaneously measuring subglacial water pressure we seek to quantify the relation between hydrological conditions at the glacier bed and the mode of basal motion.

For the 1991 field season, we devised a new sensor, dubbed a "ploughmeter", that complements our sensors for measuring subglacial strain and glacier sliding (Blake and others, 1992, in press). The device consists of a steel rod with strain gauges bonded on to it. To carry out measurements, the ploughmeter is lowered down a borehole so that its tip protrudes into subglacial sediment. Similar to an ice-entrained clast, the immersed section of the ploughmeter is dragged through subglacial sediment as a result of glacier sliding. By measuring the bending forces acting on the ploughmeter, we extract information on the mechanical conditions at the ice–bed interface. Hydrological conditions are likely to play a role because high subglacial water pressures weaken sediment and hence affect ploughing. We therefore expect the mechanical properties of the bed material to vary temporally in response to changes in the subglacial water system.

In this paper, we describe experimental techniques and the analysis of data from two ploughmeters that were installed at the bed of Trapridge Glacier during the 1991 field season. We interpret our ploughmeter observations either in terms of collisions with clasts or as a translational motion through a homogeneous, unlithified sediment layer. Theoretical analysis of the forces on the ploughmeter has yielded in-situ measurement of the effective viscosity of the deforming subglacial material.

METHODS

Description of the device

The ploughmeter (Fig. 1a) consists of a 1.54 m long solid steel rod having a diameter of 1.90 cm [0.75 in] on to which two strain gauge networks are mounted. The lower end of the rod terminates in a conical tip. The rod is sheathed in an epoxy-resin-filled, protective, vinyl tube having an inside diameter of 2.54 cm [1.0 in] and an

https://doi.org/10.3189/S0022143000003853 Published online by Cambridge University Press

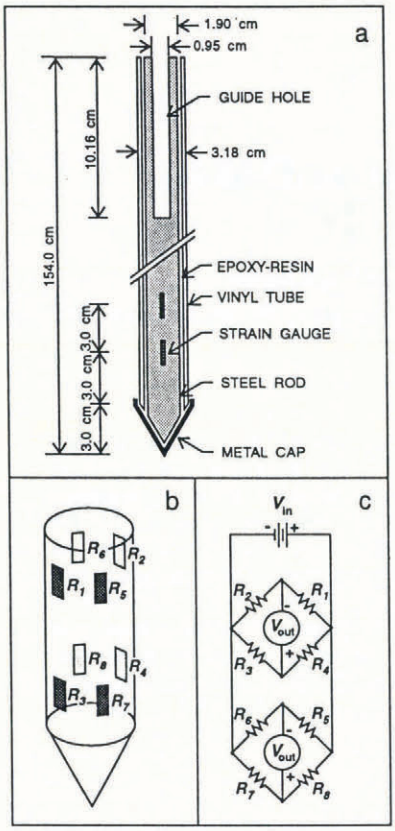

Fig. 1. a. Schematic diagram of the ploughmeter used during the 1991 field season. b. Arrangement of the eight strain guages near the tip of the steel rod. The two strain gauge networks register flexure along two perpendicular axes. c. Connection of the eight strain gauges in two full Wheatstone bridge circuits.

outside diameter of 3.18 cm [1.25 in]. Eight 20.0 mm long strain gauges (Tokyo Sokki Kenkyujo Co., Ltd; TML, PLS-20-11) are bonded, using a cyanoacrylate-based adhesive, on to a polished section near the rod tip (Fig.1b) and register flexure along two axes. A metal cap covers the conical tip to protect the sandwich construction during insertion. A 10.16 cm [4.0 in] long and 0.95 cm [0.375 in] diameter guide hole has been drilled along the axis of symmetry into the upper end of the rod and serves to guide the percussion hammer (Blake and others, 1992) that is used to insert the instrument.

To install the ploughmeter at the glacier bed, the device is lowered down a borehole and hammered into subglacial sediment. The insertion depth must be sufficient to ensure that all eight strain gauges are immersed in subglacial material. The upper section of the ploughmeter extends into the borehole and becomes pinned by the moving glacier.

Theory of the device

In the following analysis, the ploughmeter is assumed to be subjected to pure bending. Effects of any internal shear force are ignored and flexure stresses are associated only with the internal bending moment. This assumption is safe because beam length is large compared to beam diameter and thus the deformation effect of the shear force is relatively small (Byars and others, 1983, p. 272).

For elastic bending of a beam, Hooke's law states that the bending strain ϵ, defined as the fractional change in length L of the strained material, is equal to the bending stress σ divided by Young's modulus E,

$$\epsilon = \frac{\Delta L}{L} = \frac{\sigma}{E} . \tag{1}$$

The bending stress σ equals the bending moment M divided by the sectional modulus I/u, a property of the cross-sectional configuration of the beam. This relation is known as the elastic flexure equation (Byars and others, 1983, p. 305) and has the form

$$\sigma = \frac{Mu}{I} \tag{2}$$

where I represents the second moment of cross-sectional area about the horizontal centroidal axis of the beam, and u is the distance from the neutral surface (Fig. 2). On the neutral surface, fibers comprising the beam undergo no elongation or contraction when the beam is bent; if the beam has a symmetrical cross-section, this surface passes through the horizontal centroidal axis. Combining Equations (1) and (2) yields an expression for the bending strain ϵ in terms of the bending moment M,

$$\epsilon = \frac{Mu}{EI} . \tag{3}$$

The sign convention is such that strain is tensile for a positive value of u (above the neutral surface) and compressive for a negative value of u (below the neutral surface).

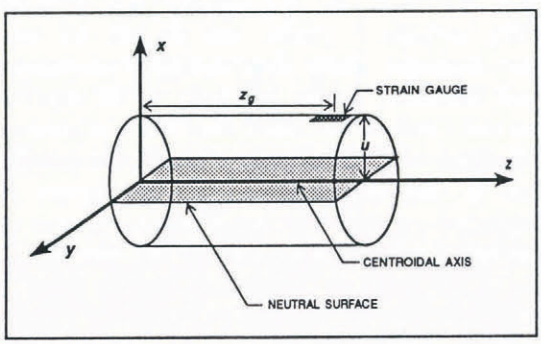

Fig. 2. Section of plougmeter showing geometrical parameters (see text for details).

Eight strain gauges (Fig. 1b) are connected as two full Wheatstone bridges (Fig. 1c). For each bridge circuit in the unstrained condition, the relationship between input voltage V_{in} and output voltage V_{out} takes the form (Murray and Miller, 1992, p. 158),

$$\left(\frac{V_{out}}{V_{in}}\right)_{unstrained} = \left[\frac{R_3}{R_3 + R_4} - \frac{R_2}{R_1 + R_2}\right] \tag{4}$$

where R_1, R_2, R_3 and R_4 are the unstrained values of strain-gauge resistance. Defining the change in resistance caused by strain as ΔR, the strained value of gauge resistance is $R + \Delta R$. Thus, for the strained condition, Equation (4) becomes

https://doi.org/10.3189/S0022143000003853 Published online by Cambridge University Press

$$\left(\frac{V_{out}}{V_{in}}\right)_{strained} = \left[\frac{R_3 + \Delta R_3}{R_3 + \Delta R_3 + R_4 + \Delta R_4} - \frac{R_2 + \Delta R_2}{R_1 + \Delta R_1 + R_2 + \Delta R_2}\right] . \quad (5)$$

The strain ϵ is related to the change in gauge resistance ΔR by

$$\epsilon = \frac{\Delta R}{RG_f} \quad (6)$$

where the constant of proportionality G_f is the gauge factor.

Combining Equations (3) and (6) yields

$$\Delta R = \frac{MuG_fR}{EI} . \quad (7)$$

The product of Young's modulus E and the second moment of area I is known as the bending modulus and is a measure of the stiffness of the beam (Byars and others, 1983, p. 306). For the ploughmeter, the bending modulus is the sum of the individual bending moduli for the three materials involved (steel, epoxy-resin and vinyl). Equation (7) relates the change in gauge resistance ΔR to the bending moment M and stiffness of the ploughmeter. The bending moment can vary with distance from the ploughmeter tip, so Equation (7) is position-dependent. Substitution of Equation (7) into Equation (5) allows calculation of the output voltages of the bridge circuits if the loading on the ploughmeter is known.

Calibration

Prior to insertion, the ploughmeter is calibrated by clamping it horizontally near the guide hole and at an intermediate point that serves as a fulcrum. Loads are then applied to the free end by hanging weights from the tip (Fig. 3a). Care must be taken to ensure that all eight strain gauges lie between the load at the tip and the fulcrum. This configuration is equivalent to a beam that is subject to a bending stress created by supports at both ends and having a load in between (Fig. 3b). The ploughmeter is calibrated using weights ranging between 1 and 30 kg that correspond to applying a load ranging from 10 to 300 N. For each load, the ploughmeter is rotated about its long axis to obtain a calibration for all possible orientations of the device with respect to the direction of glacier flow. Output voltages from each bridge circuit are fitted for each load, using least squares, to functions of the form

$$V(L_i, \phi) = A_i \cos(\phi + B_i) + C_i \quad (8)$$

where L_i are the various loads applied during the calibration, A_i are the fitted signal amplitudes at those loads, B_i are the azimuth offsets for each load, C_i are voltage offsets, ϕ represents the azimuth of the load with respect to the local coordinate system of the ploughmeter and V is the predicted voltage output. Two sets of functions of the form of Equation (8) are associated with every ploughmeter—one for each of the two bridge circuits. In a perfect device, the circuit pair would have values of B differing by exactly 90° for a given load. In practice, the orientations of the two groups of strain gauges are not exactly perpendicular and values of B are not orthogonal.

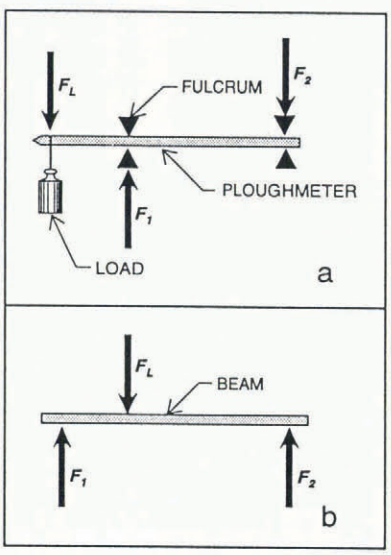

Fig. 3. a. Schematic diagram of ploughmeter calibration. b. The "three-point" load model is equivalent to the calibration configuration.

The "three-point" load model (Fig. 3b) applies to a ploughmeter installed beneath a glacier, if the ploughmeter is elastically bent by a force concentrated near the tip (the glacier bed) and a force part way up the device (the base of the ice) while the upper part of the ploughmeter is held fixed in the ice. This picture is only appropriate if forces are assumed to be small except at these three pinning points. For this case, the field data can be analyzed by computing values of L and ϕ from Equation (8) using a simplex algorithm (Press and others, 1986, p. 289) that minimizes the difference between predicted and observed output voltages. A linear regression extrapolates values of A, B and C for loads beyond the calibration range.

If, in Equation (7), we set u equal to the radius of the steel rod, while preserving the sign convention of Equation (3), and take $M(z_g) = L_i z_g$ then Equation (5) can be fitted to the calibration data set. Here, L_i are the loads used during the calibration and z_g is the distance between the point where the load is applied and the position of the strain gauge (Fig. 2). In this way, we obtain values of Young's moduli for steel, epoxy-resin and vinyl for individual ploughmeters, as well as precise resistance values R for the eight strain gauges.

For a ploughmeter installed at the glacier bed, the subglacial geometry is likely to differ substantially from that of the "three-point" calibration (Fig. 3) but the calibration remains valid. Bending forces acting on the ploughmeter are in general not concentrated near the tip but are distributed along the entire section of the ploughmeter that is immersed in subglacial sediment. We consider these distributed forces in the "Interpretation" section (below). Secondly, at the fulcrum point near the ice–bed interface, pressure melting of the borehole wall might expand the area of contact between the ice and the ploughmeter. As a result, the fulcrum load could become distributed over several centimetres. However, the bending moment $M(z_g)$ at the position z_g

https://doi.org/10.3189/S0022143000003853 Published online by Cambridge University Press

of any of the eight strain gauges is not affected as long as the strain gauge is fully immersed in subglacial material and is not located in the region of the distributed fulcrum load. Thirdly, once the ploughmeter is firmly jammed at the base of the borehole, the long axis of the ploughmeter will not necessarily be normal to the applied load at the tip. In our study, any effects of non-normality are likely to be small. Near-verticality of holes is confirmed by inclinometry. Ploughmeter length greatly exceeds hole diameter, so within each hole a ploughmeter is closely aligned with the hole axis.

FIELD OBSERVATIONS

In July 1991, two ploughmeters were inserted into sediment beneath Trapridge Glacier near the centre-line flow markers and approximately 600 m up-flow from the bulge (for location of Trapridge Glacier study area see Clarke and Blake (1991)). In the study area, the glacier has a uniform thickness of about 72 m and the surface slope is 7° in the direction of glacier flow (Blake, 1992). The insertion sites lie on a single flowline and are approximately 10 m apart. Both boreholes were unconnected to the subglacial drainage system at the time that ploughmeters were installed. The exact insertion depth of the ploughmeters into subglacial sediment is uncertain. Hydraulic excavation by the hot-water drill is believed to loosen subglacial material to a depth of several decimetres below the ice–bed interface (Blake and others, 1992). It is likely that a ploughmeter, once lowered to the bottom of the borehole, settles into this disturbed layer simply by its own weight. The measured insertion depth (14 cm for 91PL01 and 8 cm for 91PL02) therefore represents the added penetration that results from the hammering procedure. The thickness of the disturbed layer is estimated as 15–25 cm (Blake and others, 1992), so the insertion depth for the ploughmeters could range from 10 to 40 cm. During the course of our measurements, the surface velocity of Trapridge Glacier was about 10 cm d^{-1}. Observations of the deformation of boreholes reveal that for this glacier no more than 1 cm d^{-1} of the surface velocity can be accounted for by internal ice creep (Blake, 1992). The remaining 9 cm d^{-1} result from some combination of glacier sliding and sediment deformation that depends on the degree of subglacial ice–sediment coupling.

Figures 4 and 5 show 13 d of observations for ploughmeters 91PL01 and 91PL02. The data are presented in calibrated, though otherwise raw, form. An obvious feature in the force records for both ploughmeters is a gradual rise during the initial 3–5 d of observation. A diurnal signal is superimposed on the gradually rising force recorded by ploughmeter 91PL01 during the initial 3 d (Fig. 4b). Strong diurnal fluctuations in subglacial water pressure are simultaneously observed in a borehole located approximately 1 m from ploughmeter 91PL01 (Fig. 4a). At the same time, the azimuth record (Fig. 4c) indicates an apparent rotation of the ploughmeter about its long axis by up to 9°. After the initial phase, the data of ploughmeter 91PL01 display a comparatively smooth character with near-zero ploughmeter rotation. Results obtained from ploughmeter 91PL02 show a completely

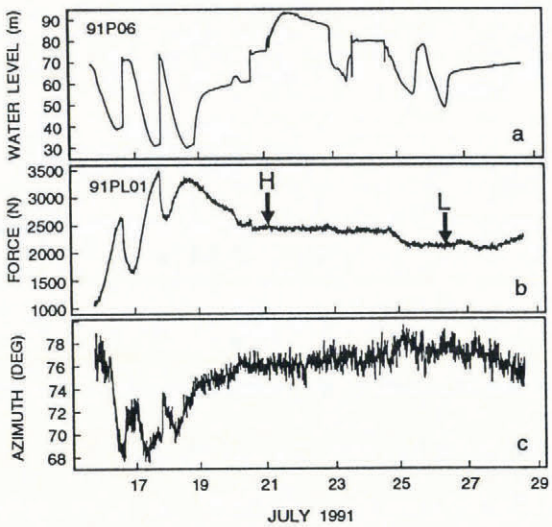

Fig. 4. Data from pressure sensor 91P06 and ploughmeter 91PL01. a. Subglacial water-pressure record. Note the diurnal signal during the initial 3 d. Super-flotation pressures correspond to a water level of more than about 63 m. b. Force record indicating load applied to the tip of the plough-meter. The arrows show the two data points that correspond to the highest (H) and lowest (L) loading during the observation period (see text for details). c. Azimuth of the load with respect to the internal coordinates of the ploughmeter.

different character. During the entire observation period, the force record (Fig. 5a) displays a sawtooth appearance, whereas the azimuth record (Fig. 5b) indicates that the ploughmeter appears to undergo a 25° back-and-forth rotation about its long axis.

If we assume that the principal direction of ploughmeter motion is down-flow, we can decompose the net force values into down-flow and cross-flow components. The azimuthal angle of the ploughmeter relative to the glacier-flow direction is a key element in this decomposition process; any disturbance on the azimuth record indicates non-zero cross-flow motion. To effect down-flow/cross-flow decomposition, we align the average azimuth to the glacier-flow direction. There could well be partitioning between rotation of the ploughmeter

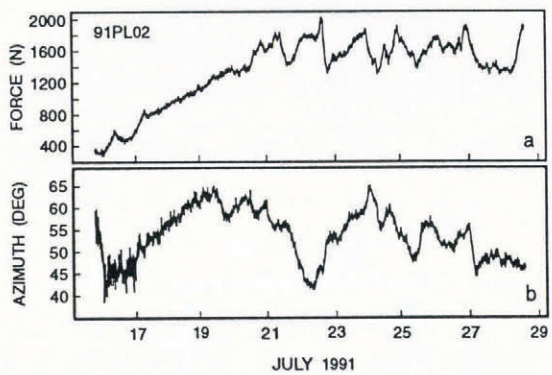

Fig. 5. Data from ploughmeter 91PL02. a. Force record indicating load applied to the tip of the ploughmeter. b. Azimuth of the load with respect to the internal coordinates of the ploughmeter.

https://doi.org/10.3189/S0022143000003853 Published online by Cambridge University Press

about its long axis and cross-flow motion but this uncertainty does not have serious consequences. Any fraction of cross-flow motion that is assigned to ploughmeter rotation reduces the cross-flow force component by that fraction, and the down-flow component will increase slightly to achieve the correct net force. However, since the partitioning has only a minor effect on the down-flow component (Fig. 6), we constrain the down-flow/cross-flow decomposition by prohibiting rotation of the ploughmeter about its long axis. Decomposition of the data of ploughmeter 91PL02 shows that there is no apparent correlation between the records of down-flow and cross-flow force components (Fig. 6c). Intervals over which a positive correlation seems to prevail are followed by intervals where the correlation seems to be negative or non-existent.

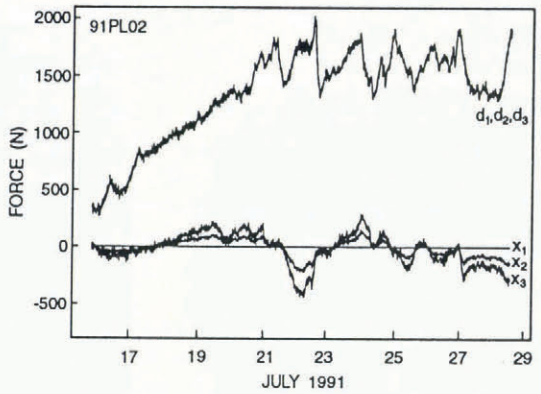

Fig. 6. Down-flow/cross-flow decomposition of the data of ploughmeter 91PL02 showing the effect of partitioning between ploughmeter rotation and cross-flow motion. Note that the partitioning has only a minor effect on the down-flow component (traces d_1, d_2 and d_3 are indistinguishable) and that cross-flow traces x_2 and x_3 differ in amplitude but have closely similar form. Trace x_1 represents 100% ploughmeter rotation. Trace x_2 represents 50% ploughmeter rotation and 50% cross-flow motion. Trace x_3 represents 100% cross-flow motion.

INTERPRETATION

For 3–5 d after installation, the ploughmeters are believed to be interacting with subglacial material that has been loosened by hydraulic excavation during hot-water drilling (Blake and others, 1992). Support for this speculation can be seen in the gradual rise of the force records of both ploughmeters. It is reasonable that this rise occurs because the ploughmeters are transported from initially loosened and disturbed material to undisturbed bed material. The smooth character of the data of ploughmeter 91PL01 might indicate that the ploughmeter was inserted into an area of the glacier bed that consists of mainly fine-grained material, but we cannot confirm this conjecture. On the other hand, the sawtooth appearance of the force record for 91PL02 suggests that the ploughmeter is interacting with a clast-rich area of the glacier bed. This explanation is supported by the fact that inserting ploughmeter 91PL02 was notably more difficult than for 91PL01, suggesting that clasts in the sediment hampered the insertion process.

A relationship between water pressure and ploughmeter–sediment interaction is unsurprising, but we have no complete explanation for the data of ploughmeter 91PL01. Vertical uplift of the glacier as a result of superflotation water pressures could explain the reduced forcing on the ploughmeter, if the ploughmeter was lifted out of the sediment. However, when pressure drops, the forcing increases, suggesting that re-insertion has occurred. Re-insertion would be difficult to explain unless the ploughmeter is firmly wedged in the hole. Alternatively, softening of the subglacial material during intervals of high water pressure could account for a reduced forcing. However, a near-instantaneous response of the ploughmeter requires rapid penetration of excess water pressure into subglacial sediment. The low-pressure diffusivity of typical subglacial sediment makes a fast response unlikely. Finally, in areas where the bed is hydraulically isolated, vertical uplift of the glacier due to an increase in subglacial water pressure should be accompanied by an essentially simultaneous decrease in the contact pressure of the ice on to the sediment. This reduction in ice-contact pressure would decrease the effective pressure in the sediment and, hence, weaken it. The apparent rotation of ploughmeter 91PL01 during periods of increased forcing might result from minor irregularities in ploughmeter geometry that could cause twisting or from pressure-induced cross-flow components of sediment deformation.

The completely different character of the ploughmeter responses inspires contrasting approaches to further analysis. Our first approach is qualitative and emphasizes the heterogeneity of subglacial sediment; the second is quantitative and emphasizes localized homogeneity. To explain the results for ploughmeter 91PL02, we shall introduce a simple model that represents collisions with clasts. To interpret the results for ploughmeter 91PL01, we shall consider the ploughmeter to be dragged through a layer of homogeneous, unlithified sediment.

Qualitative model

In an attempt to simulate collisions between individual clasts and a ploughmeter as it is dragged through sediment, we developed a simple numerical model to

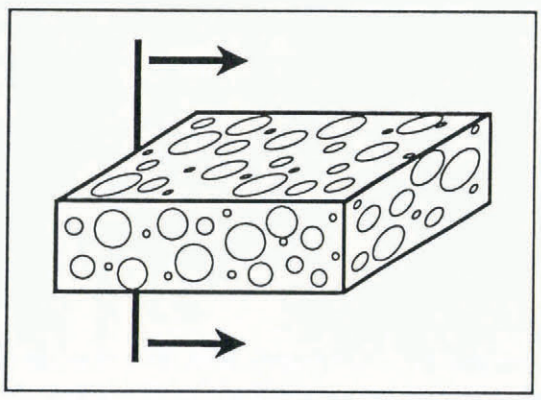

Fig. 7. Schematic diagram of the model till. The vertical line represents the ploughmeter moving through subglacial sediment.

https://doi.org/10.3189/S0022143000003853 Published online by Cambridge University Press

describe a synthetic till created by randomly filling a volume with spheres of different sizes (Fig. 7). The spheres represent clasts in a matrix of fine-grained solids and water-filled voids. We assumed a porosity of 0.3 and a clast-size distribution that is based on the granulometry of basal till from Trapridge Glacier (Clarke, 1987). Only clasts of the five largest size classes were used, corresponding to spheres of diameters 0.8–3.2 cm. Grains of smaller size were assumed to comprise the matrix of fines. However, it is interesting to note that any changes in the assumptions of porosity and size distribution do not alter the underlying idea of this simple model and have no direct influence on the qualitative nature of our conclusions. The transverse motion of a vertical line through the volume represents the ploughmeter being dragged through subglacial material. Figure 8 shows how records of down-flow and cross-flow force components are generated by considering how the path of the vertical line through the volume intersects spheres of the model till. This simple geometrical analysis is sufficient, since we are attempting to explain the character, but not the magnitudes, of the force-component records. Comparison of Figures 6c and 9 show that the records generated using this simple model display many of the features seen in the real data.

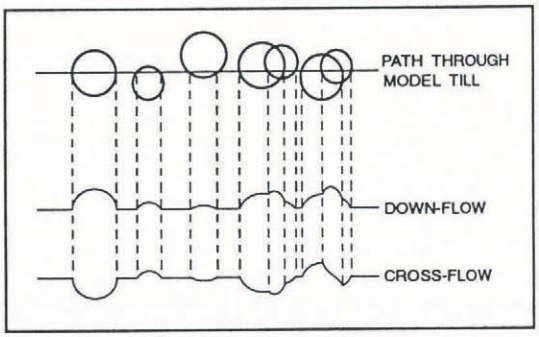

Fig. 8. Illustration of how records of down-flow and cross-flow force components are synthetically generated.

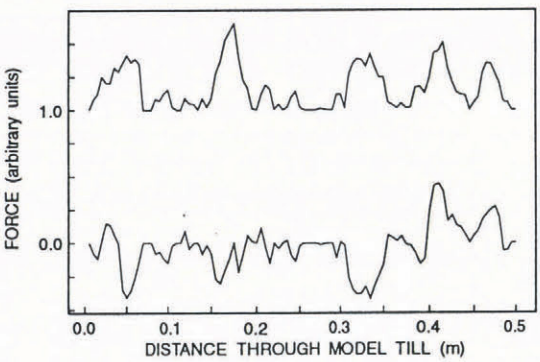

Fig. 9. Synthetically generated records of down-flow and cross-flow force components. Note the similar character to that of Figure 6.

Even though it is probable that other descriptions of ploughmeter–till interaction could lead to similar results, we feel that the above is a simple model that explains the available data. Our model also includes reasonable constraints on the nature of the till. Furthermore, it suggests directions for future effort: if till granulometry is assumed to be spatially homogeneous, then the "collision frequency", indicated by a ploughmeter, is proportional to sliding rate; on the other hand, if the sliding rate is constant, then temporal variation in the collision frequency reflects spatial variations in granulometry.

Quantitative model

For the case where the ploughmeter is dragged through a homogeneous sediment layer, the ploughmeter experiences a distributed force rather than a force concentrated near its tip. We attempt to extract information on the strength of the subglacial material by estimating how forces are distributed along the ploughmeter. However, the lack of a complete rheological description of subglacial sediment makes it difficult to calculate the force distribution on the immersed section of a ploughmeter. We therefore require a rheological model of the bed material that can provide this information. Till has been modelled as a visco-plastic material (Boulton and Hindmarsh, 1987; Alley, 1989) that is taken to have a yield strength below which no deformation occurs and above which it behaves as a viscous fluid. In our study, we separately treat the subglacial sediment as a layer of Newtonian viscous fluid and as an ideal plastic solid.

Viscosity estimate

To calculate the force distribution along the section of a ploughmeter that is immersed in sediment, we apply standard hydrodynamic theory to investigate viscous-fluid motion around a finite-moving cylinder. In this case, sediment is viewed as a Newtonian fluid having an effective viscosity μ and the ploughmeter is represented by a cylinder experiencing Stokes flow. Exact solutions for flow around finite cylinders undergoing uniform translation through a viscous fluid are unavailable but, by approximating cylinders as ellipsoids, standard solutions can be employed (Happel and Brenner, 1973, p. 227).

Under conditions where fluid inertia is negligible, the force distribution along an elongated body can be obtained as an asymptotic expansion involving the ratio of cross-sectional radius to body length (Batchelor, 1970; Cox, 1970; Tillet, 1970). For a body of length $2c$ and cross-sectional radius a that is aligned with the z axis and moving in the x direction, the force per unit length on the body can be expressed as (see Appendix for details)

$$F(z) = \mu U L(z; a, c) \tag{9}$$

where

$$L(z; a, c) = \frac{4\pi}{\ln(2c/a)\left(2\ln(2c/a) + 1\right)} \cdot \left\{ 2\ln(2c/a) - \frac{1}{2}\ln\left[\frac{a}{a(z)} \left(1 - \frac{z^2}{c^2} \right)^{\frac{1}{2}} \right] \right\} \tag{10}$$

is a characteristic length scale that incorporates the shape and dimensions of the body. In effect, the force per unit length on the body is linearly proportional to the effective fluid viscosity μ, the translational velocity U and the geometry of the body. Furthermore, the force distribution as given by Equation (9) is symmetrical about $z = 0$. If we assume a sharp ice–bed interface, we can regard it as a symmetry plane. With the origin taken to lie on this

https://doi.org/10.3189/S0022143000003853 Published online by Cambridge University Press

plane, we need only consider the negative half of the elongated body ($-c \leq z \leq 0$), which represents the section of the ploughmeter immersed in subglacial sediment.

In the case of a deforming sediment layer, shear rate is asssumed constant with depth. Accordingly, the down-flow velocity of sediment decreases linearly with distance from the ice–bed interface and the differential velocity between ploughmeter and surrounding sediment increases with depth. For this case, where the ploughmeter is moving through an already-shearing sediment layer, the velocity U in Equation (9) represents the differential velocity between the ploughmeter and the sediment and becomes a function of z. The thickness of the deformable sediment layer beneath Trapridge Glacier is assumed to be 0.5 m (Blake and Clarke, 1989).

To calculate the force distribution along the section of a ploughmeter immersed in subglacial sediment (Equation (9)), we approximate the shape of the ploughmeter as either an ellipsoid (Equation (A9)) or a cylinder (Equation (A12)). While the ellipsoid assumption likely underestimates the forces in the lower section of the ploughmeter, end effects at the flat faces of the cylinder greatly overestimate the forces near the conical tip. We expect that the true result lies somewhere between that yielded by the ellipsoidal and the cylindrical approximations, and regard the ellipsoid as a better overall representation of the ploughmeter.

Once the force distribution on the immersed section of the ploughmeter is known, the bending moment $M(z_g)$ at the position z_g of a strain gauge can easily be calculated according to

$$M(z_g) = \int_{-c}^{z_g} F(z)(z_g - z)\mathrm{d}z = \mu \int_{-c}^{z_g} U(z)L(z; a, c)(z_g - z)\mathrm{d}z . \quad (11)$$

Here, z_g is a negative value, since the strain gauge is located below the ice–bed interface, and c corresponds to the depth to which the ploughmeter is immersed in sediment. It is assumed that the viscosity μ is constant with depth in the sediment. Equation (11) is substituted into Equation (7) for all eight strain gauges of a ploughmeter. An estimate of μ can be obtained by minimizing (Press and others, 1986, p. 283) the objective function

$$f(\mu) = \sum_{i=1}^{2} \left[\left(\frac{V_{out}}{V_{in}} \right)_{observed,i} - \left(\frac{V_{out}}{V_{in}} \right)_{predicted,i} \right]^2 . \quad (12)$$

The sum in Equation (12) is taken over the two bridge circuits. The data set of ploughmeter 91PL01 supplies the observed voltage ratios and the predicted voltage ratios are calculated using Equation (5).

By this method, the apparent viscosity of subglacial sediment has been calculated as a function of ploughmeter insertion depth for three different styles of basal motion (Fig. 10). Figure 10a and b represents the two end-member cases of 100% glacier sliding and 100% bed deformation. In Figure 10c, we assume that 50% of the 9 cm d^{-1} basal velocity is due to glacier sliding and 50% is due to bed deformation. Using the record of ploughmeter

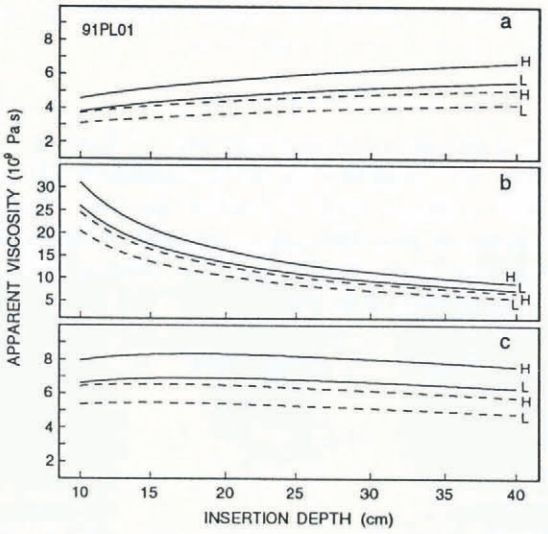

Fig. 10. Apparent viscosity of subglacial sediment as a function of insertion depth of ploughmeter 91PL01 for three different styles of basal motion. Solid lines indicate ellipsoidal approximation. Dashed lines indicate cylindrical approximation. Highest and lowest loading (see Fig. 4b) is denoted by H and L, respectively. a. 100% glacier sliding. b. 100% sediment deformation in a 0.5 m thick layer. c. 50% glacier sliding and 50% bed deformation.

91PL01, the calculations were carried out for two data points that correspond to the highest and lowest loading during the observation period (see arrows labelled H and L in Figure 4b). We have not included the initial 5 d of the record, because we believe these represent a start-up phase that does not characterize ploughmeter interaction with an undisturbed subglacial bed.

Results are shown for both ellipsoidal and cylindrical shapes. We note that the apparent viscosity calculated for the ellipsoid is greater than that for the cylinder, because forces near the end of a cylinder exceed those near the tip of an ellipsoid. Within the uncertainties and assumptions listed above, we can limit the viscosity estimate to a spread of one order of magnitude. The 100% deformation model yields an upper bound on apparent viscosity in the range 5.6×10^9–3.1×10^{10} Pa s; the 100% sliding model yields a lower bound of 3.0×10^9–6.6×10^9 Pa s. These estimates of Trapridge Glacier sediment viscosity are consistent with those of Blake (1992) and Blake and Clarke (1989).

Yield-strength estimate

Following the analysis by Humphrey and others (1993), we can estimate the plastic yield strength of subglacial material by considering plastic flow around a stiff cylinder. We approximate the cylinder by a flat and long rigid indenter of width equal to the diameter of the ploughmeter. If we define the problem in plane strain, thereby ignoring end effects, the stress that the indenter exerts on the semi-infinite plastic body on to which it is pressed, is uniformly distributed and can be expressed as (Hill, 1971, p. 340)

$$\sigma = (2 + \pi)k \quad (13)$$

where k is the plastic yield strength of the material. To close the wake left by a positive indenter, Humphrey and

https://doi.org/10.3189/S0022143000003853 Published online by Cambridge University Press

others (1993) introduced a negative indenter of equal strength and obtained the expression

$$F = 4a(2 + \pi)k \tag{14}$$

where a is the radius of the ploughmeter. If Equation (14) describes the dragging of the ploughmeter through subglacial sediment, then F denotes the force per unit length acting on the immersed section of the ploughmeter.

With this force distribution, the bending moment $M(z_g)$ can be calculated as

$$\begin{aligned} M(z_g) &= \int_{-c}^{z_g} F(z_g - z)\mathrm{d}z \\ &= 4a(2 + \pi)k \int_{-c}^{z_g} (z_g - z)\mathrm{d}z \end{aligned} \tag{15}$$

where z_g denotes the position of the strain gauge. The development is closely analogous to that of the previous section and proceeds by substituting Equation (15) into Equation (7) for all eight strain gauges of a ploughmeter. Again, an expression similar to Equation (12) is minimized, analyzing the same two data points that were used to obtain a viscosity estimate, to calculate an estimate of k. The plastic yield strength obtained by this method is 48–57 kPa.

Discussion

The rheology of subglacial material is doubtless more complex than our simple model rheologies and should probably incorporate pore-water pressure, deformation history and heterogeneity of the material. Nevertheless, the simple models give us some indication of the ability of subglacial material to resist deformation. Estimates of plastic yield strength and effective viscosity derived in this study can be compared to the applied shear stress beneath Trapridge Glacier. Assuming a plane-slab geometry, the mean basal shear stress beneath our study site is 77 kPa. If subglacial sediment were plastic, then the inferred yield strength is about 70% of the applied shear stress. On the other hand, for the case of Newtonian viscous behaviour, the basal strain rate can be calculated as about 33 year^{-1}. Here, glacier sliding is neglected and the entire basal motion of 9 cm d^{-1} is assumed to result from uniform shear deformation in a 0.5 m thick sediment layer. If the deforming layer was Newtonian viscous and resisted the basal shear stress of 77 kPa, then the 33 year^{-1} strain rate represents a viscosity of 4×10^{10} Pa s. The viscosity inferred in our study is up to an order of magnitude lower. Thus, for the viscous and plastic rheologies, the estimates of sediment strength yielded by the ploughmeter analysis suggest that the deformational resistance of the bed is comparable to, but somewhat less than, that required to ensure mechanical stability in this region of Trapridge Glacier.

Results of previous work on in situ measurements of the strength of deforming sediment differ from those obtained in our study. Humphrey and others (1993) obtained estimates of sediment viscosity and plastic yield strength by analyzing the plastic deformation of a drill stem that became stuck in the bed of Columbia Glacier, Alaska. They reported viscosities (2×10^8–5×10^8 Pa s) and yield strengths (5.5–13 kPa) that are as much as one order of magnitude lower than our estimates. At the same time, the basal shear stress beneath Columbia Glacier (100 kPa) is about 30% greater than that calculated for Trapridge Glacier. Results from tests of basal till from beneath Ice Stream B (Kamb, 1991) indicated a plastic-like behaviour and resulted in estimates of the yield strength (1.6–2.0 kPa) that also tend to be softer than those derived here. Ice Stream B has a significantly lower basal shear stress yet higher flow rate (Alley and others, 1987) than Trapridge Glacier, consistant with a weaker subglacial sediment. Viscosities calculated from the results of the work done by Boulton and Hindmarsh (1987) beneath Breidamerkurjökull in Iceland are generally an order of magnitude higher (10^{10}–10^{11} Pa s) than our estimates. The Breidamerkurjökull observations and those on Trapridge Glacier are not directly comparable. The Breidamerkurjökull measurements were carried out in a tunnel penetrating very thin ice near the glacier margin, where mechanical and hydrological conditions might be unusual. Furthermore, natural variations in sediment composition can account for different stiffnesses.

Our analysis of the strength of subglacial material includes a number of assumptions. These are listed and briefly discussed as follows:

1. Solutions for creeping motion of a viscous fluid around solid bodies are based on the assumption that the bodies are immersed in a homogeneous and incompressible Newtonian fluid. In effect, the deforming bed is treated as a continuum that has no internal structure and it is assumed that a no-slip boundary exists at the ploughmeter surface. Thus clast-scale interaction processes are neglected.

2. The results of the slender-body theory (see Appendix) are only applicable for long bodies possessing large length-to-diameter ratios c/a. To get some sense of the error introduced by applying slender-body theory to short objects, we compared the drag calculated using Oberbeck's formula (Equation (A3)) to the slender-body result (Equation (A11)). For $c/a = 6.3$ (corresponds to an insertion depth of the ploughmeter of $c = 10$ cm), the discrepancy is about 0.19%, which reduces to about 0.009% for $c/a = 25$ (corresponds to $c = 40$ cm).

3. Motion of the ploughmeter through ice has been completely neglected. This assumption is probably safe, since the protective vinyl tube coating the ploughmeter also acts as a thermal insulator and suppresses the regelation mechanism.

4. Hydrological and mechanical perturbations of the subglacial environment, caused by the presence of a water-filled borehole, have been neglected.

CONCLUDING REMARKS

Our instrument allows for continuous and long-term observation of mechanical processes at the ice–bed interface. One of the main attractions of the ploughmeter is that it is robust, simple in design and inexpensive to build. The device should therefore prove useful for studying evolving conditions beneath normal and surge-type glaciers.

https://doi.org/10.3189/S0022143000003853 Published online by Cambridge University Press

The 1991 measurements suggest that, across the bed of Trapridge Glacier, either the granulometry of subglacial sediment is not uniform or ice–sediment coupling varies significantly. If one assumes that, at the scale of 10 m, lateral variations in sliding velocity are insignificant, ploughmeter 91PL01 appears to have been immersed in a region of the bed that predominantly consists of fine-grained material, whereas ploughmeter 91PL02 seems to interact with a clast-rich sediment. On the other hand, spatial variations in basal-glacier motion could account for different behaviours of ploughmeter–sediment interaction.

We have suggested that the deformation resistance of the bed is comparable to but less than that needed to balance the applied basal shear stress. This conclusion is non-robust because it depends on which rheology is adopted.

ACKNOWLEDGEMENTS

We thank the Natural Sciences and Engineering Research Council of Canada for funding this research and the University of British Columbia for providing postgraduate fellowship support. Our field work was conducted in Kluane National Park. We thank the Park Superintendent and staff for their co-operation and the Government of the Yukon Territory for issuing a "Scientists and Explorers Licence". The authors wish to acknowledge the technical assistance provided by K. D. Schreiber in the construction of the ploughmeters. This research profited from the intellectual contributions of B. S. Waddington. Advice, assistance and comments were also gratefully received from E. W. Blake, D. B. Stone and T. Murray. We also acknowledge N. R. Iverson and P. U. Clark for improving the manuscript.

REFERENCES

Alley, R. B. 1989. Water-pressure coupling of sliding and bed deformation: II. Velocity-depth profiles. *J. Glaciol.*, **35**(119), 119–129.

Alley, R. B., D. D. Blankenship, C. R. Bentley, and S. T. Rooney. 1987. Till beneath Ice Stream B. 3. Till deformation: evidence and implications. *J. Geophys. Res.*, **92**(B9), 8921–8929.

Batchelor, G. K. 1970. Slender-body theory for particles of arbitrary cross-section in Stokes flow. *J. Fluid Mech.*, **44**(3), 419–440.

Blake, E. W. 1992. The deforming bed beneath a surge-type glacier: measurement of mechanical and electrical properties. (Ph.D. thesis, University of British Columbia.)

Blake, E. W. and G. K. C. Clarke. 1989. In situ bed strain measurements beneath a surge-type glacier. *EOS*, **70**(43), 1084. [Abstract.]

Blake, E. W., G. K. C. Clarke and M. C. Gérin. 1992. Tools for examining subglacial bed deformation. *J. Glaciol.*, **38**(130), 388–396.

Blake, E. W., U. H. Fischer and G. K. C. Clarke. In press. Direct measurement of sliding at the glacier bed. *J. Glaciol.*

Boulton, G. S. and R. C. A. Hindmarsh. 1987. Sediment deformation beneath glaciers: rheology and geological consequences. *J. Geophys. Res.*, **92**(B9), 9059–9082.

Boulton, G. S. and A. S. Jones. 1979. Stability of temperate ice caps and ice sheets resting on beds of deformable sediment. *J. Glaciol.*, **24**(90), 29–43.

Byars, E. F., R. D. Snyder and H. L. Plants. 1983. *Engineering mechanics of deformable bodies. Fourth edition.* New York, Harper and Row.

Clarke, G. K. C. 1987. Subglacial till: a physical framework for its properties and processes. *J. Geophys. Res.*, **92**(B9), 9023–9036.

Clarke, G. K. C. and E. W. Blake. 1991. Geometric and thermal evolution of a surge-type glacier in its quiescent state: Trapridge Glacier, Yukon Territory, Canada, 1969–89. *J. Glaciol.*, **37**(125), 158–169.

Cox, R. G. 1970. The motion of long slender bodies in a viscous fluid. Part 1. General theory. *J. Fluid Mech.*, **44**(4), 791–810.

Engelhardt, H. F., W. D. Harrison and B. Kamb. 1978. Basal sliding and conditions at the glacier bed as revealed by bore-hole photography. *J. Glaciol.*, **20**(84), 469–508.

Engelhardt, H., N. Humphrey and B. Kamb. 1990a. Borehole geophysical observations on Ice Stream B, Antarctica. *Antarct. J. U.S.*, **25**(5), 80–82.

Engelhardt, H., N. Humphrey, B. Kamb and M. Fahnestock. 1990b. Physical conditions at the base of a fast moving Antarctic ice stream. *Science*, **248**(4951), 57–59.

Happel, J. and H. Brenner. 1973. *Low Reynolds number hydrodynamics. Second edition.* Leyden, Noordhoff International Publishing.

Hill, R. 1971. *The mathematical theory of plasticity.* Oxford, Oxford University Press.

Humphrey, N. F., H. F. Engelhardt, M. Fahnestock and B. Kamb. 1993. Characteristics of the bed of the lower Columbia Glacier, Alaska. *J. Geophys. Res.*, **98**(B1), 837–846.

Kamb, B. 1991. Rheological nonlinearity and flow instability in the deforming bed mechanism of ice stream motion. *J. Geophys. Res.*, **96**(B10), 16,585–16,595.

Kamb, B. and H. Engelhardt. 1989. Flow mechanics of West Antarctic ice streams: observations by borehole geophysics. *EOS*, **70**(43), 1081. [Abstract.]

Kamb, B. and E. LaChapelle. 1964. Direct observation of the mechanism of glacier sliding over bedrock. *J. Glaciol.*, **5**(38), 159–172.

Kohler, J. and R. Proksch. 1991. *In-situ* measurement of subglacial till deformation beneath Storglaciären, N. Sweden. *EOS*, **72**(44), 158. [Abstract.]

Murray, W. M. and W. R. Miller. 1992. *The bonded electrical resistance strain gage.* New York, Oxford University Press.

Oberbeck, A. 1876. Über stationäre Flüssigkeitsbewegungen mit Berücksichtigung der inneren Reibung. *Crelles J.*, **81**, 62–80.

Oseen, C. W. 1927. *Neuere Methoden and Ergebnisse in der Hydrodynamik.* Leipzig, Akademische Verlagsgesellschaft M.B.H.

Press, W. H., B. P. Flannery, S. A. Teukolsky and W. T. Vetterling. 1986. *Numerical recipes: the art of scientific computing.* Cambridge, Cambridge University Press.

Schlichting, H. 1979. *Boundary-layer theory. Seventh edition.* New York, McGraw-Hill.

Stokes, G. G. 1851. On the effect of the internal friction of fluids on the motion of pendulums. *Trans. Cambridge Philos. Soc.*, **9**, 8–106.

Tillett, J. P. K. 1970. Axial and transverse Stokes flow past slender axisymmetric bodies. *J. Fluid Mech.*, **44**(3), 401–417.

The accuracy of references in the text and in this list is the responsibility of the authors, to whom queries should be addressed.

APPENDIX

FORCES ON AN ELONGATED BODY IN STOKES FLOW

For very small Reynolds numbers, inertial forces are negligible compared with the pressure and viscous forces. Thus, for a body having surface S at rest in an incompressible fluid which at infinity is undergoing a uniform translational motion at velocity $\mathbf{U}$, the velocity $\mathbf{v}$ and pressure p in the fluid satisfy the creeping motion equations (Schlichting, 1979, p. 112)

$$\begin{aligned} \mu\nabla^2\mathbf{v} &= \nabla p \\ \nabla \cdot \mathbf{v} &= 0\,, \end{aligned} \tag{A1}$$

with the boundary conditions

$$\begin{aligned} \mathbf{v} &= 0 \quad \text{on} \quad S \\ \mathbf{v} &\to \mathbf{U} \quad \text{as} \quad \mathbf{x} \to \infty \end{aligned} \tag{A2}$$

https://doi.org/10.3189/S0022143000003853 Published online by Cambridge University Press

where μ is the fluid viscosity and $\mathbf{x}$ is the position vector of a general point. Oberbeck (1876) solved this problem in the case of an ellipsoid and obtained the total drag exerted on such a body. In particular, for an elongated ellipsoid of revolution having semi-axes a and c with $c > a$, Oberbeck's formula for fluid motion perpendicular to the symmetry axis leads to a drag of magnitude

$$D = \frac{16\pi\mu a U}{\left[\frac{c/a}{(c/a)^2 - 1} + \frac{2(c/a)^2 - 3}{[(c/a)^2 - 1]^{\frac{3}{2}}} \ln\left(\frac{c}{a} + \sqrt{(c/a)^2 - 1}\right)\right]} . \tag{A3}$$

For large length-to-diameter ratios c/a, Equation (A3) reduces to

$$D = \frac{8\pi\mu c U}{\ln(2c/a) + 0.5} . \tag{A4}$$

Also, in the limit, as the length-to-diameter ratio c/a approaches unity, Oberbeck's solution (Equation (A3)) yields Stokes' law

$$D = 6\pi\mu a U , \tag{A5}$$

which describes the total drag of a sphere of radius a undergoing uniform translation through a viscous fluid (Stokes, 1851).

To obtain the force distribution along an elongated axisymmetric body moving perpendicularly through a viscous fluid, we follow the treatment by Batchelor (1970), which is based on slender-body theory for Stokes flow with negligible inertial forces. The key idea is that it is possible to approximate the body by a suitably chosen system of forces, known as "Stokeslets", distributed along the symmetry axis. The effect of these Stokeslets is to disturb the uniform motion of the surrounding fluid. For a force $\mathbf{F}$ applied at the origin in an infinite body of fluid, the velocity at the point $\mathbf{x}$ in flow with negligible inertial forces is (Oseen, 1927)

$$\frac{F_j}{8\pi\mu}\left(\frac{\delta_{ij}}{|\mathbf{x}|} + \frac{x_i x_j}{|\mathbf{x}|^3}\right) \tag{A6}$$

where μ is the fluid viscosity. Thus, if Stokeslets are distributed over the portion $-c < x_3 < c$ of the x_3 axis so that the line density of the applied force is $\mathbf{F}(x_3)$, the resulting fluid velocity at point $\mathbf{x}$ is

$$v_i(\mathbf{x}) = \frac{1}{8\pi\mu}\int_{-c}^{c}\left[\frac{F_i(x_3')}{((x_3 - x_3')^2 + r^2)^{\frac{1}{2}}} + \frac{(x_i - x_i')(x_j - x_j')F_j(x_3')}{((x_3 - x_3')^2 + r^2)^{\frac{3}{2}}}\right] dx_3' \tag{A7}$$

where $x_1' = x_2' = 0$ and $r^2 = x_1^2 + x_2^2$. This distribution of Stokeslets represents the disturbance motion of an axisymmetric body of length $2c$, and points on the body surface are given by $r = a(x_3)$, where $a(x_3)$ is the radius of the body as a function of x_3 and $a(x_3)/c$ is small compared to unity. If we choose the axes of reference so that the body is stationary, the undisturbed velocity is $-\mathbf{U}$. This case corresponds to the translational motion of the body with velocity $\mathbf{U}$ through a fluid at rest at infinity.

In order to satisfy the no-slip condition of Equation (A2), the resultant fluid velocity $\mathbf{v} - \mathbf{U}$ must be zero at the body surface. Thus, the unknown function $\mathbf{F}(x_3)$, representing the Stokeslet strength distribution, must be chosen so that the velocity due to the line of Stokeslets cancels the undisturbed velocity at all points on the surface of the body. It is possible to use a line distribution of Stokeslets as a means of satisfying the no-slip condition at points on the surface only if the body is slender. Thus, the integral Equation (A7) with $\mathbf{v} = \mathbf{U}$ at $r = a(x_3)$ can be approximated by an asymptotic expansion in terms of the ratio of cross-sectional radius to body length $(a(x_3)/c \to 0)$ (Batchelor, 1970; Cox, 1970; Tillet, 1970). If the undisturbed velocity $\mathbf{U}$ is in the x_1 direction, the force per unit length on the body can be expressed as

$$\mathbf{F}(x_3) = \frac{4\pi\mu U}{\ln(2c/a)(2\ln(2c/a) + 1)} \cdot \left\{2\ln(2c/a) - \frac{1}{2}\ln\left[\frac{a}{a(x_3)}\left(1 - \frac{x_3^2}{c^2}\right)^{\frac{1}{2}}\right]\right\} \tag{A8}$$

where a is the radius of the body at $x_3 = 0$.

In the particular case of an ellipsoidal body (Batchelor, 1970)

$$\frac{a(x_3)}{a} = \left(1 - \frac{x_3^2}{c^2}\right)^{\frac{1}{2}} \quad \text{for} \quad -c \le x_3 \le c , \tag{A9}$$

and Equation (A8) reduces to

$$\mathbf{F}(x_3) = \frac{4\pi\mu U}{\ln(2c/a) + 0.5} . \tag{A10}$$

To obtain the total drag of the ellipsoid, we integrate Equation (A10) over the length of the body. This yields

$$D = \int_{-c}^{c} \mathbf{F}(x_3)\, dx_3 = \frac{8\pi\mu c U}{\ln(2c/a) + 0.5} , \tag{A11}$$

which corresponds to Oberbeck's result given in Equation (A4). In the case of a cylindrical body, we substitute (Cox, 1970)

$$\frac{a(x_3)}{a} = 1 \quad \text{for} \quad -c \le x_3 \le c \tag{A12}$$

into Equation (A8).

MS received 26 June 1992 and in revised form 24 November 1992